Aalborg Universitet

AALBORG UNIVERSITY

Magnetoplasmon resonances in nanoparticles

Pedersen, Thomas Garm

Link to publication from Aalborg University

Magnetoplasmon resonances in nanoparticles

Thomas Garm Pedersen ●[*]

Department of Materials and Production, Aalborg University, DK-9220 Aalborg Øst, Denmark

Nanoparticle plasmon resonances can be controlled using external magnetic fields or internal magnetization. The modified resonance condition is complicated, however, by the induced anisotropy of the dielectric response. Working within the electrostatic regime, we formulate a simple eigenvalue problem for the magnetoplasmon resonances. Subsequently, a semianalytical perturbative solution valid for weak magnetic fields is obtained for the resonance shift. We apply the approach to Drude metal nanodisks and show that resonance shifts are generally smaller than for nanospheres and nanoellipsoids. Finally, energy-dependent effective masses in Dirac materials are shown to reduce shifts compared to free-electron-like materials.

I. INTRODUCTION

Plasmon resonances in metallic nanoparticles are of importance for a range of phenomena and applications including sensing [1,2] and photovoltaics [3–5]. Depending on the application, plasmon resonances in the infrared, visible, or even ultraviolet may be desired. For a nanoparticle, the spectral position of the resonance is determined by a number of factors. Primarily, material properties are of importance. Hence, the overall spectral scale is set by the conduction electron plasma frequency that, in turn, increases with carrier density and inverse effective mass. Similarly, materials are characterized by their interband screening, which reduces resonance frequencies. Thus, metals such as Al with high carrier density and low screening lead to resonances in the ultraviolet [6] while doped semiconductors [7] and graphene [8] support infrared plasmon due to their low plasma frequencies. Second, particle shape affects plasmon resonances. In the electrostatic or nonretarded regime, however, scale invariance means that plasmon resonances are independent of absolute size [9–12]. Hence, the resonance of all small spheres of a particular material are identical. In disks and ellipsoids, resonances split into separate short- and long-axis modes. This leads to a certain degree of freedom when designing nanoparticles to support resonances in specific spectral ranges. Moreover, coupling between modes in neighboring particles can shift resonances into desired spectral locations [12].

In passive plasmonics, resonances are completely fixed by nanoparticle shape and composition. In contrast, active plasmonics allows for tunable resonances. An important case is found in two-dimensional materials, in which gating can control plasmons via carrier density [8]. Similarly, physical movement of a particle can be applied to shift resonances [13]. Finally, it has long been realized that an external magnetic field (or internal magnetization) leads to a split of plasmon modes due to cyclotron motion of electrons [14–19]. Such magnetoplasmons have been envisioned for dedicated sensing applications [14,16–18]. In this respect, it is important to understand the effect of particle shape and composition on the splitting. For carriers in a parabolic band with effective mass m_e, the characteristic quantity when placed in a magnetic field B is the cyclotron frequency $\omega_c = eB/m_e$. In fact, in the electrostatic regime, the resonances of spheres and ellipsoids all split by precisely $\pm\frac{1}{2}\omega_c$ independent of particle elongation [20–23]. Hence, for this class of particle shapes, geometry cannot be applied to tune the shift. As we will show in the present work, however, this conclusion is only valid for spheres and ellipsoids. Hence, also plasmon splitting can be tuned by particle shape. This is highly relevant for practical applications since these often rely on nanodisks rather than ellipsoids or spheres [14,17,18].

In the present work, we formulate the magnetoplasmon resonance condition in the electrostatic regime as an eigenvalue problem using the surface charge prescription of Mayergoyz and co-workers [9–12]. The problem is significantly simplified for cylindrically symmetric particles in a magnetic field aligned along the symmetry axis [24–27]. For fields of arbitrary strength, a complicated resonance condition is found. However, for relatively small fields, i.e., whenever $\omega_c \ll \omega$ for an excitation of frequency ω, we find that vertical resonances polarized along the symmetry axis are unaltered while a simplified resonance condition is found for horizontal modes. A compact perturbation expression is then found to completely capture the magnetoplasmon resonance shift. Thus, only the solution to the zero-field problem is required to evaluate the magnetoplasmon resonances.

II. MAGNETOPLASMON RESONANCES

As mentioned above, the problem is greatly simplified in the case of cylindrical symmetry. We therefore consider the geometry in Fig. 1. Here, a nanoparticle with a rotational symmetry axis z is assumed and the homogeneous and static external magnetic field is aligned with the symmetry axis $\vec{B} = B\hat{z}$. In general, internal magnetization along the z axis leads to an equivalent problem. In the absence of an external field, the nanoparticle is assumed isotropic with a frequency-dependent
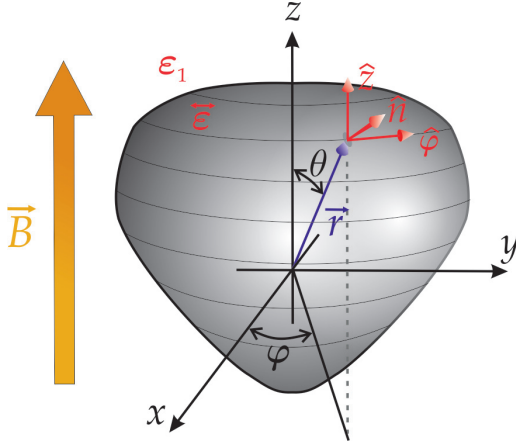
*tgp@mp.aau.dk

FIG. 1. Cylindrically symmetric metal nanoparticle in magnetic field aligned along the symmetry axis. The optically anisotropic particle is embedded in an isotropic medium with dielectric constant ε_1.

dielectric constant $\varepsilon(\omega)$. In this case, the tensorial dielectric response in the presence of the field is of the gyrotropic form [28],

$$
\overset{\leftrightarrow}{\varepsilon} = \begin{pmatrix} \varepsilon_{xx} & \varepsilon_{xy} & 0 \\ -\varepsilon_{xy} & \varepsilon_{xx} & 0 \\ 0 & 0 & \varepsilon_{zz} \end{pmatrix}. \tag{1}
$$

We will return to the field dependence of the tensor elements below. In addition, we take the particle to be embedded in a homogeneous medium with dielectric constant ε_1. In the surface charge approach, charges $\sigma(\vec{r}')$ at position $\vec{r}'$ produce a potential at $\vec{r}$ proportional to $\sigma(\vec{r}')/|\vec{r} - \vec{r}'|$. In turn, in the electrostatic approximation, the electric field is proportional to

$$
\vec{g}(\vec{r}, \vec{r}') = -\nabla \frac{1}{|\vec{r} - \vec{r}'|} = \frac{\vec{r} - \vec{r}'}{|\vec{r} - \vec{r}'|^3}. \tag{2}
$$

This integral kernel is singular, however, and the associated field depends on the manner, in which the limit $\vec{r} \to \vec{r}'$ is taken. Accordingly, for $\vec{r}'$ and $\vec{r}$ on the particle surface, the fields on either side are given by the surface integral [9–12]

$$
\vec{\mathcal{E}}^{\text{out/in}}(\vec{r}) = \frac{1}{4\pi\varepsilon_0} \oint \vec{g}(\vec{r}, \vec{r}')\sigma(\vec{r}')dS' \pm \hat{n}\frac{\sigma(\vec{r})}{2\varepsilon_0}, \tag{3}
$$

where $+$ and $-$ go with the fields infinitesimally outside and inside the particle, respectively, $\hat{n}$ is the outward unit normal vector, and dS' is an infinitesimal surface element at position $\vec{r}'$. Importantly, here and throughout, principle-value integrals are assumed. Hence, the discontinuity is entirely contained in the last term, which reflects the electromagnetic boundary conditions, i.e., the discontinuity of the normal component. For a cylindrically symmetric particle, $\hat{n} = (n_x \cos\varphi, n_x \sin\varphi, n_z)$ with azimuthal angle φ; cf. Fig. 1. Projecting onto the normal direction and defining $\mathcal{E}_a^{\text{out/in}} \equiv \hat{a} \cdot \vec{\mathcal{E}}^{\text{out/in}}(\vec{r})$, the boundary condition is then

$$
\varepsilon_1 \mathcal{E}_n^{\text{out}}(\vec{r}) = \hat{n} \cdot \overset{\leftrightarrow}{\varepsilon} \cdot \vec{\mathcal{E}}^{\text{in}}(\vec{r}) = \varepsilon_{xx}\mathcal{E}_n^{\text{in}}(\vec{r}) + \varepsilon_{xy}n_x\mathcal{E}_\varphi^{\text{in}}(\vec{r})
$$
$$
+ (\varepsilon_{zz} - \varepsilon_{xx})n_z\mathcal{E}_z^{\text{in}}(\vec{r}). \tag{4}
$$

Combined with Eq. (3), this means that

$$
\sigma(\vec{r}) = \frac{1}{2\pi(\varepsilon_{xx}n_x^2 + \varepsilon_{zz}n_z^2 + \varepsilon_1)} \oint \{(\varepsilon_{xx} - \varepsilon_1)g_n(\vec{r}, \vec{r}')
$$
$$
+ \varepsilon_{xy}g_\varphi(\vec{r}, \vec{r}') + (\varepsilon_{zz} - \varepsilon_{xx})g_z(\vec{r}, \vec{r}')\}\sigma(\vec{r}')dS', \tag{5}
$$

where we have defined the projected Green's functions via $g_a(\vec{r}, \vec{r}') = p_a\hat{a} \cdot \vec{g}(\vec{r}, \vec{r}')$ with prefactors $p_n = 1$, $p_z = \hat{n} \cdot \hat{z} = n_z$, and $p_\varphi = \hat{n} \cdot (\hat{x}\hat{y} - \hat{y}\hat{x}) \cdot \hat{\varphi} = n_x$. Also, we use the convention that unprimed quantities in integrals such as the normal vector components $n_{x,z}$ are evaluated at position $\vec{r}$ while primed ones are evaluated at $\vec{r}'$. Equation (5) is the eigenvalue problem to be solved for a gyrotropic nanoparticle. In the isotropic case $\varepsilon_{xx} = \varepsilon_{zz} = \varepsilon$ and $\varepsilon_{xy} = 0$, this leads to the usual eigenvalue problem with $\lambda = (\varepsilon - \varepsilon_1)/(\varepsilon + \varepsilon_1)$ as eigenvalue [9–12,24–26].

We now specialize to the cases of vertical and horizontal polarization, i.e., excitation by vertically or horizontally polarized fields. In the former case, cylindrical symmetry ensures a surface charge independent of φ. In the latter, modes varying as $\exp(\pm i\varphi)$ are sought. In the case of vertical polarization $\sigma(\vec{r}) = \sigma(\theta)$, we define $G_a^{(v)}(\theta, \theta') = (2\pi)^{-1}\int_0^{2\pi} g_a(\vec{r}, \vec{r}')d\varphi'$. The nanoparticle surface is parametrized by $r = r(\theta)$ and $r' = r(\theta')$. Performing the azimuthal integral using elementary geometrical relations we find

$$
G_n^{(v)}(\theta, \theta') = [n_z(r\cos\theta - r'\cos\theta') + n_x r\sin\theta]
$$
$$
\times F_{0,1}(x, y) - n_x r'\sin\theta' F_{1,1}(x, y),
$$
$$
G_z^{(v)}(\theta, \theta') = n_z(r\cos\theta - r'\cos\theta')F_{0,1}(x, y),
$$
$$
G_\varphi^{(v)}(\theta, \theta') = 0, \tag{6}
$$

where $x = r^2 + r'^2 - 2rr'\cos\theta\cos\theta'$, $y = -2rr'\sin\theta\sin\theta'$, and we have introduced the functions

$$
F_{m,n}(x, y) \equiv \frac{1}{2\pi} \int_0^{2\pi} \frac{\cos^m\varphi \, d\varphi}{(x + y\cos\varphi)^{(2n+1)/2}}. \tag{7}
$$

Explicit expressions for the lowest (m, n) cases and computational prescriptions can be found in Ref. [24]. The surface area element is $dS = S(\theta)d\theta d\varphi$ with area function [26] $S(\theta) = r^2(\theta)\sin\theta/(n_x\sin\theta + n_z\cos\theta)$. Hence, upon integration over φ',

$$
\sigma(\theta) = \frac{1}{\varepsilon_{xx}n_x^2 + \varepsilon_{zz}n_z^2 + \varepsilon_1} \int_0^\pi \{(\varepsilon_{xx} - \varepsilon_1)G_n^{(v)}(\theta, \theta')
$$
$$
+ (\varepsilon_{zz} - \varepsilon_{xx})G_z^{(v)}(\theta, \theta')\}\sigma(\theta')S(\theta')d\theta'. \tag{8}
$$

The case of horizontal polarization is slightly more complicated due to the off-diagonal ε_{xy} response coupling the field components. The general eigenmode is of the form $\sigma(\vec{r}) = \sigma_\pm(\theta)\exp(\pm i\varphi)$ and we therefore define real and imaginary parts

$$
G_a^{(h)}(\theta, \theta') = \frac{1}{2\pi} \int_0^{2\pi} g_a(\vec{r}, \vec{r}')\cos(\varphi - \varphi')d\varphi',
$$
$$
F_a^{(h)}(\theta, \theta') = \frac{1}{2\pi} \int_0^{2\pi} g_a(\vec{r}, \vec{r}')\sin(\varphi - \varphi')d\varphi'. \tag{9}
$$

Hence, with three possible vectors, a total of six projected Green's functions result. However, after integration only three

nonvanishing components remain:

$$G_n^{(h)}(\theta, \theta') = [n_z(r\cos\theta - r'\cos\theta') + n_x r \sin\theta]$$
$$\times F_{1,1}(x, y) - n_x r' \sin\theta' F_{2,1}(x, y),$$

$$G_z^{(h)}(\theta, \theta') = n_z(r\cos\theta - r'\cos\theta')F_{1,1}(x, y),$$

$$F_\varphi^{(h)}(\theta, \theta') = n_x r' \sin\theta'[F_{0,1}(x, y) - F_{2,1}(x, y)]. \quad (10)$$

In terms of these, the eigenproblems for $\sigma_\pm(\theta)$ read

$$\sigma_\pm(\theta) = \frac{1}{\varepsilon_{xx}n_x^2 + \varepsilon_{zz}n_z^2 + \varepsilon_1} \int_0^\pi \left\{ (\varepsilon_{xx} - \varepsilon_1)G_n^{(h)}(\theta, \theta') \right.$$
$$+ (\varepsilon_{zz} - \varepsilon_{xx})G_z^{(h)}(\theta, \theta') \pm i\varepsilon_{xy}F_\varphi^{(h)}(\theta, \theta') \right\}$$
$$\times \sigma_\pm(\theta')S(\theta')d\theta'. \quad (11)$$

Generally, Eqs. (8) and (11) can be solved by sweeping over frequency. This is a rather cumbersome task, however. We therefore now utilize the assumption that the material is isotropic in the absence of a magnetic field such that $\varepsilon_{xx} = \varepsilon_{zz} = \varepsilon$ and $\varepsilon_{xy} = 0$ at $B = 0$. In the presence of a weak field [17,29], $\varepsilon_{zz} - \varepsilon_{xx} = O(B^2)$ while $\varepsilon_{xy} = O(B)$. Hence, retaining only first-order corrections, we find for the vertical case

$$\sigma(\theta) = \frac{\varepsilon - \varepsilon_1}{\varepsilon + \varepsilon_1} \int_0^\pi G_n^{(v)}(\theta, \theta')\sigma(\theta')S(\theta')d\theta', \quad (12)$$

while for the horizontal case

$$\sigma_\pm(\theta) = \frac{\varepsilon - \varepsilon_1}{\varepsilon + \varepsilon_1} \int_0^\pi \left\{ G_n^{(h)}(\theta, \theta') \pm \frac{i\varepsilon_{xy}}{\varepsilon - \varepsilon_1}F_\varphi^{(h)}(\theta, \theta') \right\}$$
$$\times \sigma_\pm(\theta')S(\theta')d\theta'. \quad (13)$$

In these simplified relations, ε is now the zero-field isotropic response. Hence, the vertical eigenproblem is unaffected by the magnetic field but the horizontal case is still perturbed by the off-diagonal correction. This demonstrates that, to linear order, magnetoplasmon shifts are absent for vertical eigenmodes in cylindrically symmetric geometries. For the horizontal modes, the unperturbed problem reads

$$\sigma_0(\theta) = \lambda_0 \int_0^\pi G_n^{(h)}(\theta, \theta')\sigma_0(\theta')S(\theta')d\theta'. \quad (14)$$

Here, $\sigma_0(\theta)$ is the unperturbed eigenfunction and $\lambda_0 = [\varepsilon(\omega_0) - \varepsilon_1]/[\varepsilon(\omega_0) + \varepsilon_1]$ the unperturbed eigenvalue that, in turn, provides the unperturbed resonance ω_0. In addition, one may define the adjoint (or left) eigenfunction $\sigma_0^\dagger(\theta)$ via

$$\sigma_0^\dagger(\theta') = \lambda_0 \int_0^\pi G_n^{(h)}(\theta, \theta')\sigma_0^\dagger(\theta)S(\theta)d\theta. \quad (15)$$

Note the change in integration variable here. We normalize these such that $\int_0^\pi \sigma_0^\dagger(\theta)\sigma_0(\theta)S(\theta)d\theta = 1$. Importantly, these unperturbed eigenproblems are easily solved using standard routines.

In the presence of the magnetic field, the resonance frequency shifts from ω_0 to ω corresponding to an eigenvalue $\lambda = [\varepsilon(\omega) - \varepsilon_1]/[\varepsilon(\omega) + \varepsilon_1]$. In relatively weak magnetic fields, perturbation theory allows for a straightforward solution in terms of the zero-field eigenmode, which is easily

obtained. Collecting first-order terms in Eq. (13), we find

$$\lambda \approx \lambda_0 \pm \frac{i\varepsilon_{xy}(\omega_0)\lambda_0(\lambda_0 - 1)}{2\varepsilon_1}$$
$$\times \int_0^\pi \int_0^\pi \sigma_0^\dagger(\theta)F_\varphi^{(h)}(\theta, \theta')\sigma_0(\theta')S(\theta')d\theta'd\theta. \quad (16)$$

We stress that the perturbative regime is defined by $\omega_c \ll \omega$. However, for resonances in the visible and applying the free-electron mass $m_e = m_0$, a ratio of $\omega_c/\omega = 10^{-3}$ still requires a substantial field of $B \approx 17$T and, thus, the perturbative result remains accurate in nearly all cases.

III. APPLICATION TO NANODISKS

The theory formulated so far is quite general. To provide quantitative results for realistic geometries, we now consider a screened free-electron-like metal. The interband dielectric constant is ε_∞ and to all orders in the cyclotron frequency $\omega_c = eB/m_e$ [17,29]

$$\varepsilon_{xx}(\omega) = \varepsilon_\infty - \frac{\omega_p^2}{\omega}\frac{\omega + i\gamma}{(\omega + i\gamma)^2 - \omega_c^2},$$

$$\varepsilon_{zz}(\omega) = \varepsilon_\infty - \frac{\omega_p^2}{\omega(\omega + i\gamma)}, \quad (17)$$

$$\varepsilon_{xy}(\omega) = \frac{i\omega_c\omega_p^2}{\omega}\frac{1}{(\omega + i\gamma)^2 - \omega_c^2}.$$

Here, ω_p is the plasma frequency and a phenomenological line broadening γ was included. We now adopt these results to the perturbation approach by retaining only first-order effects of the magnetic field. As mentioned above, there is no linear contribution to the diagonal anisotropy and, in the collision-less limit, $\varepsilon_{xx} = \varepsilon_{zz} \approx \varepsilon$ with $\varepsilon(\omega) = \varepsilon_\infty - \omega_p^2/\omega^2$ and $\varepsilon_{xy}(\omega) \approx i\omega_c\omega_p^2/\omega^3$. The perturbation result Eq. (16) then directly translates into resonances given by $\omega = \omega_0 \pm \frac{1}{2}\Delta\omega$ with

$$\Delta\omega \approx \omega_c\frac{\lambda_0}{\lambda_0 - 1} \int_0^\pi \int_0^\pi \sigma_0^\dagger(\theta)F_\varphi^{(h)}(\theta, \theta')\sigma_0(\theta')S(\theta')d\theta'd\theta. \quad (18)$$

The unperturbed solution $\{\sigma_0, \lambda_0\}$ is completely independent of material properties and, in fact, Eq. (14) is a scale-invariant equation, which is indifferent to the absolute particle size. Material properties only enter whenever the eigenvalue is translated into a resonance frequency via $\lambda_0 = [\varepsilon(\omega_0) - \varepsilon_1]/[\varepsilon(\omega_0) + \varepsilon_1]$. Hence, the normalized shift $\Delta\omega/\omega_c$ is actually independent of the material properties and entirely determined by geometry. The absolute shift is obviously enhanced in materials with a low effective mass via the cyclotron frequency. Also, it is seen that the split resonances are always symmetrically positioned above and below ω_0. If losses are retained via γ in Eqs. (17), the resonance expression Eq. (18) is multiplied by a factor $\Gamma = [1 + i\gamma/(2\omega_0)]^{-1}$. Since $|\Gamma| < 1$, the presence of losses will reduce the magnitude of the shift slightly.

As a technologically relevant example [14,17,18], we consider nanodisks such as the one shown in the lower inset of Fig. 2. Here, the geometry is defined by height h and width w and the edges are rounded by quarter circles with radius
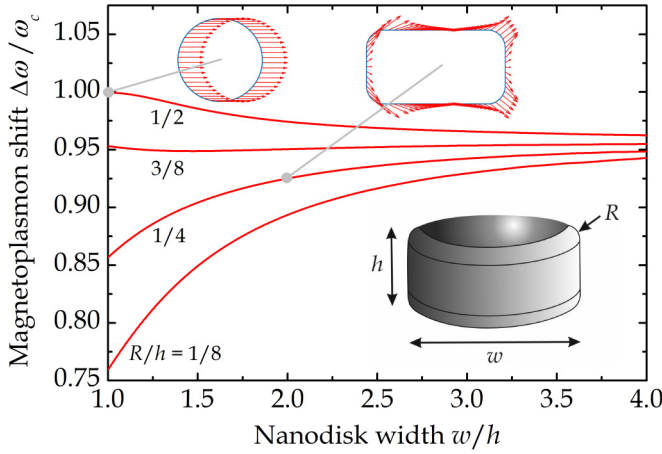
FIG. 2. Normalized magnetoplasmon shift for the nanodisk shown in the lower inset. Different curves correspond to different rounding radii on the edges. Surface fields for two cases are shown at the top.
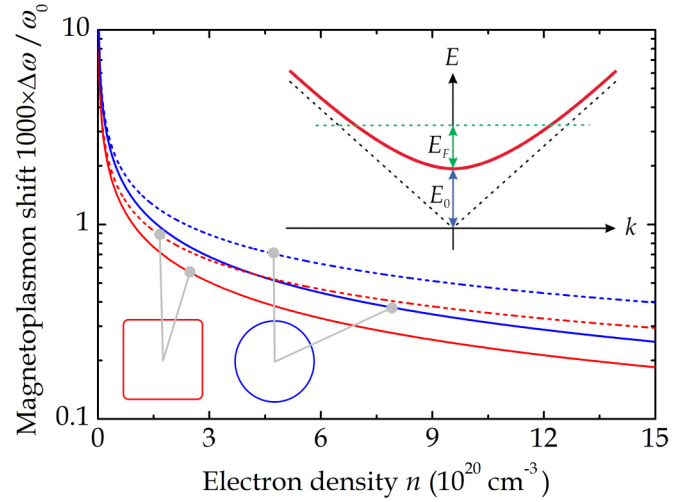

FIG. 3. Relative magnetoplasmon shift vs density for ZnO disks (red curves) and spheres (blue curves) in air taking $B = 1$T. For both geometries, Dirac and free-electron dispersion results are illustrated by solid and dashed lines, respectively. The upper inset shows the Dirac energy dispersion.

$R \leqslant h/2$ producing a smooth profile with continuously varying surface parametrization $r(\theta)$ and normal vectors $\vec{n}$. Due to the above-mentioned scale invariance, we fix h and measure w and R in units of h. We also note that for $2R = w = h$ the shape is that of a perfect sphere. We solve Eqs. (14) and (15) by discretizing on an equidistant angular grid using up to 3000 grid points. The singular diagonal elements of the Green's functions are found but integrating between grid points using a 50 times denser grid designed to avoid the singularity.

The shift $\Delta\omega/\omega_c$ is shown for various nanodisk geometries in Fig. 2. It is seen from the figure that $\Delta\omega/\omega_c$ is generally below unity and, intriguingly, seems to approach a common value ~0.95 for wide disks irrespective of rounding radius. We emphasize that these are completely general curves that apply to any material that can be accurately modelled by the screened Drude model Eq. (18). Moreover, a shift of $\Delta\omega/\omega_c = 1$ is found in the limit of a perfect sphere $2R = w = h$. Also, it is known that for disks of vanishing thickness $w/h \to \infty$, such as graphene quantum dots, a shift $\Delta\omega/\omega_c = 1$ is obtained [30]. For finite height h, Fig. 2 shows that the normalized shift is generally less than unity. In agreement with previous work [16,20–23], we find that $\Delta\omega = \omega_c$ for all spheres and ellipsoids.

To rationalize the difference between disks and spheres, it is instructive to consider the local surface field, i.e., Eq. (3) evaluated immediately inside the nanoparticle surface. The azimuthal behavior of the local field is dictated by the incident excitation. However, even for strictly horizontal excitation aligned along $\theta = \pi/2$, the local field may, in general, display a more complicated θ behavior. Thus, the local field may point in directions deviating significantly from $\theta = \pi/2$, in particular near corners. The exceptions to this are precisely spheres and ellipsoids. As shown in the left-most upper inset in Fig. 2, the surface field is strictly horizontal for a sphere. Hence, there is no coupling to the z component of the dielectric constant. In contrast, a nanodisk (right-most upper inset) is characterized by local fields with a significant z component near the corners. We now recall that only the (x, y) motion is affected by the magnetic field to first order, while the vertical

dielectric response ε_{zz} is unaffected. Hence, nanoparticles characterized by local fields contained in the (x, y) plane are expected to feel the magnetic effects more strongly than those with a significant z component of the response. It may be conjectured, then, that $\Delta\omega/\omega_c \leqslant 1$ for arbitrary shapes and that only ellipsoids (and spheres) exhaust the inequality. The physical interpretation is that only spheres and ellipsoids allow all electrons to move in a plane perpendicular to the magnetic field, thereby maximizing the Lorentz force. This is of consequence for design of nanoparticles having a large magnetoplasmonic response. Presumably, no shape is better than ellipsoids in the electrostatic limit, at least for Drude metals.

IV. DIRAC MATERIALS

The previous section only applied to free-electron-like materials with a parabolic dispersion. In certain technologically relevant doped semiconductors such as ZnO [7], as well as graphene and phosphorene [31], the dispersion is of the Dirac type. For gapped Dirac materials, the dispersion can be written as [7] $E = \sqrt{E_0^2 + \hbar^2 k^2 E_0/m_e}$. Hence, the band structure is that of a hyperboloid, which is approximately parabolic at small k with an effective mass m_e. However, as k increases, the dispersion approaches a linear band with asymptotic velocity $v = \sqrt{E_0/m_e}$. This behavior can be viewed as an effective mass that increases with energy. Hence, high-energy electrons with large effective masses are expected to feature a small cyclotron frequency and, consequently, a smaller magneto-plasmon shift than electrons near the bottom of the band. The constant E_0 is the minimum energy, i.e., band edge, measured from the intersection of the asymptotes as shown in Fig. 3. We will now assume a homogeneous and isotropic three-dimensional Dirac material, for which semiclassical Boltzmann theory predicts an unperturbed dielectric constant

given by

$$\varepsilon(\omega) = \varepsilon_\infty + \frac{e^2}{4\pi^3 \varepsilon_0 \omega^2} \int v_x^2 f'(E) d^3 k. \quad (19)$$

Here, we again neglect losses and band velocities should be evaluated as $\hbar v_i = dE/dk_i$. Moreover, $f'(E)$ is the energy derivative of the Fermi-Dirac distribution and we have added a constant interband term ε_∞. Similarly, to first order in the magnetic field, the optical Hall response becomes

$$\varepsilon_{xy}(\omega) = -\frac{ie^3 B}{4\pi^3 \varepsilon_0 \hbar \omega^2} \int f'(E) v_y \left\{ \frac{\partial v_x}{\partial k_x} v_y - \frac{\partial v_x}{\partial k_y} v_x \right\} d^3 k.$$
$$(20)$$

At low electron density n, these response functions resemble their free-electron counterparts as the occupied portion of the band structure is nearly parabolic. However, at high density, marked deviations are found. We measure the Fermi level E_F from the band edge as seen in Fig. 3. In terms of the low-density plasma frequency $\omega_p = (e^2 n/\varepsilon_0 m_e)^{1/2}$ and cyclotron frequency $\omega_c = eB/m_e$, we find with $\eta \equiv (1 + E_F/E_0)^{-1}$

$$\varepsilon(\omega) = \varepsilon_\infty - \frac{\omega_p^2}{\omega^2} \eta, \quad \varepsilon_{xy}(\omega) = \frac{i\omega_c \omega_p^2}{\omega^3} \eta^2. \quad (21)$$

Hence, $\eta \leqslant 1$ is a measure of the deviation from free-electron-like behavior, which is only expected whenever $\eta \approx 1$. To relate η to the electron density n, we note that $E_F = \sqrt{E_0^2 + \hbar^2 k_F^2 E_0/m_e}$ with Fermi wave vector $k_F = (3\pi^2 n)^{1/3}$. Thus, it follows that $\eta = [1 + (n/n_0)^{2/3}]^{-1/2}$ with characteristic density $n_0 = (m_e E_0)^{3/2}/(3\pi^2 \hbar^3) \approx 1.2 \times 10^{20} \text{cm}^{-3}$ obtained by fitting to full band structure data for ZnO [7]. Significant fingerprints of the Dirac dispersion are expected whenever $n \sim n_0$. In Fig. 3, we illustrate this fact by investigating the ratio $\Delta\omega/\omega_0$ between shift and resonance frequency. Solving the eigenvalue relation $\lambda_0 = [\varepsilon(\omega_0) - \varepsilon_1]/[\varepsilon(\omega_0) + \varepsilon_1]$, we see that the unperturbed resonance is

$$\omega_0 = \frac{\omega_p \sqrt{\eta}}{\sqrt{\varepsilon_\infty + \varepsilon_1 \frac{\lambda_0 + 1}{\lambda_0 - 1}}}. \quad (22)$$

Similarly, a perturbation analysis using Eq. (21) readily shows that for a Dirac material, the shift Eq. (18) is replaced by

$$\Delta\omega \approx \omega_c \eta \frac{\lambda_0}{\lambda_0 - 1} \int_0^\pi \int_0^\pi \sigma_0^\dagger(\theta) F_\varphi^{(h)}(\theta, \theta')$$
$$\times \sigma_0(\theta') S(\theta') d\theta' d\theta. \quad (23)$$

It follows that an analysis of magnetoplasmons in Dirac materials is just as simple as in the free-electron-like case. Below, we evaluate $\Delta\omega/\omega_0 \propto \eta^{1/2}$ as a function of density and compare to the parabolic case $\eta = 1$ using the expressions derived above.

In the numerical results shown in Fig. 3, we have assumed a field of $B = 1$ T and consider spheres as well as disks with $w = h$ and $R = h/16$, i.e., a nearly square cross section. Also, for ZnO [32], $\varepsilon_\infty \approx 3.85$ and we take $\varepsilon_1 = 1$ corresponding to nanoparticles in air. In the limit of small density, the unperturbed plasmon resonance ω_0 vanishes while the shift $\Delta\omega$ remains finite. Hence, their ratio diverges as $n \to 0$ but around the characteristic density $n \approx n_0$, a ratio of order $\Delta\omega/\omega_0 \approx 10^{-3}$ is found. In the high-density regime $n > n_0$, noticeable differences between Dirac and free-electron materials are observed. As $\Delta\omega/\omega_0 \propto \eta^{1/2}$, Dirac materials clearly support a smaller magnetoplasmon shift for a given density. At the largest density $n = 15 \times 10^{20}$ cm^{-3} in Fig. 3, this reduction is by a factor $\eta^{1/2} \approx 2.5$. Hence, we conclude that highly doped semiconductors with a pronounced Dirac energy dispersion are less sensitive to magnetic fields than might be expected from their generally small effective mass at the band edge.

V. SUMMARY

We have presented a theory of magnetoplasmon resonances in cylindrically symmetric nanoparticle geometries valid within the electrostatic limit. A resonance condition for general gyrotropic dielectric response is formulated. For weak magnetic fields, a perturbation expression for the shift of plasmon resonances is found. This allows for a simple evaluation of the magnetoplasmon response that, furthermore, is universally valid for all Drude-like materials. The theory has been applied to nanodisks, which are generally found to be less sensitive to magnetic fields than ellipsoids and spheres. Finally, magnetoplasmon shifts in materials with a Dirac-like energy dispersion are shown to be smaller than those of free-electron-like structures.

[1] M. Moskovits, Rev. Mod. Phys. **57**, 783 (1985).

[2] S. Lal, S. Link, and N. J. Halas, Nat. Photon. **1**, 641 (2007).

[3] C. Hägglund, M. Zäch, and B. Kasemo, Appl. Phys. Lett. **92**, 013113 (2008).

[4] J. S. Biteen, N. S. Lewis, and H. A. Atwater, Appl. Phys. Lett. **88**, 131109 (2006).

[5] K. R. Catchpole and A. Polman, Opt. Express **16**, 21793 (2008).

[6] M. W. Knight, N. S. King, L. Liu, H. O. Everitt, P. Nordlander, and N. J. Halas, ACS Nano **8**, 834 (2014).

[7] J. Jung and T. G. Pedersen, J. Appl. Phys. **113**, 114904 (2013).

[8] A. N. Grigorenko, M. Polini, and K. S. Novoselov, Nat. Photon. **6**, 749 (2012).

[9] I. D. Mayergoyz, D. R. Fredkin, and Z. Zhang, Phys. Rev. B **72**, 155412 (2005).

[10] I. D. Mayergoyz and Z. Zhang, IEEE Trans. Magn. **42**, 759 (2006).

[11] I. D. Mayergoyz, Z. Zhang, and G. Miano, Phys. Rev. Lett. **98**, 147401 (2007).

[12] Z. Zhang, I. D. Mayergoyz, N. A. Gumerov, and R. Duraiswami, IEEE Trans. Magn. **43**, 1465 (2007).

[13] W. Cheng, M. J. Campolongo, J. J. Cha, S. J. Tan, C. C. Umbach, D. A. Muller, and D. Luo, Nat. Mater. **8**, 519 (2009).

[14] V. Bonanni, S. Bonetti, T. Pakizeh, Z. Pirzadeh, J. Chen, J. Nogués, P. Vavassori, R. Hillenbrand, J. Åkerman, and A. Dmitriev, Nano Lett. **11**, 5333 (2011).

[15] E. Melander, E. Östman, J. Keller, J. Schmidt, E. T. Papaioannou, V. Kapaklis, U. B. Arnalds, B. Caballero, A. García-Martín, J. C. Cuevas, and B. Hjörvarsson, Appl. Phys. Lett. **101**, 063107 (2012).

[16] F. Pineider, G. Campo, V. Bonanni, C. de Julián Fernández, G. Mattei, A. Caneschi, D. Gatteschi, and C. Sangregorio, Nano Lett. **13**, 4785 (2013).

[17] G. Armelles, A. Cebollada, A. García-Martín, and M. U. González, Adv. Opt. Mater. **1**, 10 (2013).

[18] N. Maccaferri, K. E. Gregorczyk, T. V. De Oliveira, M. Kataja, S. Van Dijken, Z. Pirzadeh, A. Dmitriev, J. Åkerman, M. Knez, and P. Vavassori, Nat. Commun. **6**, 6150 (2015).

[19] B. Han, X. Gao, L. Shi, Y. Zheng, K. Hou, J. Lv, J. Guo, W. Zhang, and Z. Tang, Nano Lett. **17**, 6083 (2017).

[20] J. K. Furdyna, S. Goettig, J. Mycielski, and W. Trzeciakowski, Phys. Rev. B **31**, 7714 (1985).

[21] S. Goettig and W. Trzeciakowski, Phys. Rev. B **31**, 7726 (1985).

[22] R. P. Devaty, Phys. Rev. B **38**, 7972 (1988).

[23] G. Weick and D. Weinmann, Phys. Rev. B **83**, 125405 (2011).

[24] J. Jung, T. G. Pedersen, T. Søndergaard, K. Pedersen, A. N. Larsen, and B. B. Nielsen, Phys. Rev. B **81**, 125413 (2010).

[25] J. Jung, T. G. Pedersen, T. Søndergaard, K. Pedersen, A. Nylandsted Larsen, and B. Bech Nielsen, Phys. Status Solidi RRL **4**, 292 (2010).

[26] T. G. Pedersen, J. Jung, T. Søndergaard, and K. Pedersen, Opt. Lett. **36**, 713 (2011).

[27] C. Pecharromán, J. Pérez-Juste, G. Mata-Osoro, L. M. Liz-Marzán, and P. Mulvaney, Phys. Rev. B **77**, 035418 (2008).

[28] G. W. Ford and S. A. Werner, Phys. Rev. B **18**, 6752 (1978).

[29] Z. Yu, G. Veronis, Z. Wang, and S. Fan, Phys. Rev. Lett. **100**, 023902 (2008).

[30] W. Wang, S. P. Apell, and J. M. Kinaret, Phys. Rev. B **86**, 125450 (2012).

[31] T. G. Pedersen, Phys. Rev. B **95**, 235419 (2017).

[32] Z.-C. Jin, I. Hamberg, and C. G. Granqvist, J. Appl. Phys. **64**, 5117 (1988).